
Multi-objective Design Optimization and Control Strategy for Digital Hydraulically Driven Knee Exoskeleton

Rituraj* and Rudolf Scheidl

*Institute of Machine Design and Hydraulic Drives, Johannes Kepler University,
Linz, Austria*

E-mail: rituraj.rituraj@jku.at; rudolf.scheidl@jku.at

**Corresponding Author*

Received 01 September 2022; Accepted 03 November 2022;
Publication 29 April 2023

Abstract

This article presents a multi-objective design optimization strategy to determine an optimal design of digital hydraulically driven knee exoskeleton. To satisfy the overall goal of compact and lightweight design, four key design objectives are defined. Via genetic algorithm based multi-objective optimization technique, the pareto-optimal set of designs is determined and the trade-offs between the design objectives are analysed. Via decisions based on component availability and user-comfort, the dimensionality of the pareto-front is reduced to two and an exoskeleton design is selected that offers a good compromise between the design objectives.

For the actuation of the exoskeleton, an energy efficient control strategy is proposed which consists of using passive control during the stance phase and simplified model predictive control during the swing phase. The operation of

International Journal of Fluid Power, Vol. 24.2, 271–298.

doi: 10.13052/ijfp1439-9776.2425

© 2023 River Publishers

the chosen knee exoskeleton design and the control strategy is investigated via numerical simulations. The results indicate that the exoskeleton successfully tracks the desired knee motion and delivers the required knee torque.

Keywords: Knee exoskeleton, hydraulic drives, digital hydraulics, design optimization.

1 Introduction

Exoskeletons are wearable devices that facilitate the motion of human limbs with an enhanced strength. Such devices have a wide range of applications. In medical treatment, these devices help the patients in motion assistance and regaining the power of their limbs. In industries, they assist workers in carrying heavy loads without risking fatigue and injuries. Soldiers, firefighters, and rescue workers can also use these devices to carry heavy equipment over long distances.

In last few decades, several exoskeletons with a wide range of designs, operating principles and applications have been developed [1]. Among them, the powered exoskeletons have been found to be primarily dominated by electro-mechanical drives [2]. However, the hydraulically actuated exoskeletons present an attractive alternative due to their several potential advantages:

- High force density: This allows the reduction of the mass and space occupied by the exoskeleton device.
- Easy energy recuperation: This improves the system efficiency and ensures long battery life of the power source.
- Damping behaviour: This allows the realization of smooth and natural motion patterns.
- Motion locking without power supply: This further improves the operational efficiency of the device.

Despite these potentials, the development of such hydraulic devices remains at a nascent stage with respect to the following key challenges: lightweight and energy-efficient design, fast and efficient control, and design in view of the availability of appropriate hydraulic components.

Two of the earliest hydraulically actuated exoskeletons were developed at University of California, Berkeley called Berkeley's lower extremity exoskeleton [3–5] and by Sarcos Research Corporation called XOS [6]. The former used linear hydraulic actuators, whereas the latter used rotary

hydraulic actuators. In recent years, key improvements in the design and control of hydraulically actuated exoskeletons have been made [7–9]. However, these exoskeleton devices use traditional hydraulic drives with resistance control which is known for its poor energy efficiency and thus, the device requires a larger energy source.

In last two decades, digital hydraulics has emerged as an innovative technology that offers several advantages such as high efficiency, force density, precision, and robustness [10]. An early application of such a technology to exoskeleton devices was the ELEBOT exoskeleton developed by Cao et al. [11] which used switching controlled two-way valves.

In last few years, the authors' research group has been working on various ideas to realize a digitally driven knee exoskeleton device. Holl et al. proposed a knee exoskeleton design [2, 12] powered by a digital hydraulic cylinder where 3/3 way switching valves were used to set the pressure in each of the four chambers of the digital cylinder. The transformation from the linear motion of the cylinder to the angular motion of the knee was achieved by a 4-bar linkage mechanism. The main drawback of this design is the expensiveness associated with the multi-chamber cylinders needed to realize the digital cylinder concept.

In a recent work, the authors have developed a novel design of knee exoskeleton [13]. The design consists of a unique linkage mechanism that allows digital actuation of the knee exoskeleton with simple hydraulic cylinders rather than a multi-chamber cylinder. The mechanism further allows the handling of peak knee torque requirements in a gait cycle with moderate hydraulic system pressures.

Nevertheless, the challenges related to compact, lightweight, and energy-efficient design and fast and efficient control still need to be tackled. To this end, in this work, an optimization study is conducted to determine an optimal exoskeleton design that satisfies the requirements of compactness, low weight, and high energy efficiency. Furthermore, an energy efficient strategy to control the exoskeleton actuation is proposed. The performance of this control strategy is investigated by a numerical model of the knee exoskeleton and human limb motion.

This article is divided into 7 sections including this introduction section. In Section 2, the knee exoskeleton design developed by the authors is presented. Next, Section 3 provides the details of the optimization study conducted to obtain the optimal kinematic structure. In Section 4, the control strategy of exoskeleton actuation is described. The numerical model used to analyse the behaviour of the exoskeleton device is presented in Section 5.

Next, the results from the numerical model are presented in Section 6. Finally, Section 7 provides the summary and key conclusions drawn from this work.

2 Knee Exoskeleton Design

The design of the knee exoskeleton device is shown in Figure 1. The device consists of the thigh and shank parts. The angular motion between these two parts is accomplished via two mechanisms. Each mechanism consists of a hydraulic cylinder and connecting rod in addition to the thigh and shank parts. The pin joint between the hydraulic cylinder and connecting rod is constrained to move along a guided path. This guide curve is realized via grooves on the guide plate (one groove for each mechanism). The shape of this guide curve is determined by the transmission ratio of the mechanism (Section 2.2) and the dimensions of the links in the mechanism.

2.1 Hydraulic Drive

The digital hydraulic system driving the knee exoskeleton device is shown in Figure 2. Miniature hydraulic cylinders from HAWE Micro Fluid GmbH [14] are used in the design. Furthermore, 2/2-way micro-valves from Tampere University [15] are used to connect each of the chambers of the cylinders to the pressure source and tank.

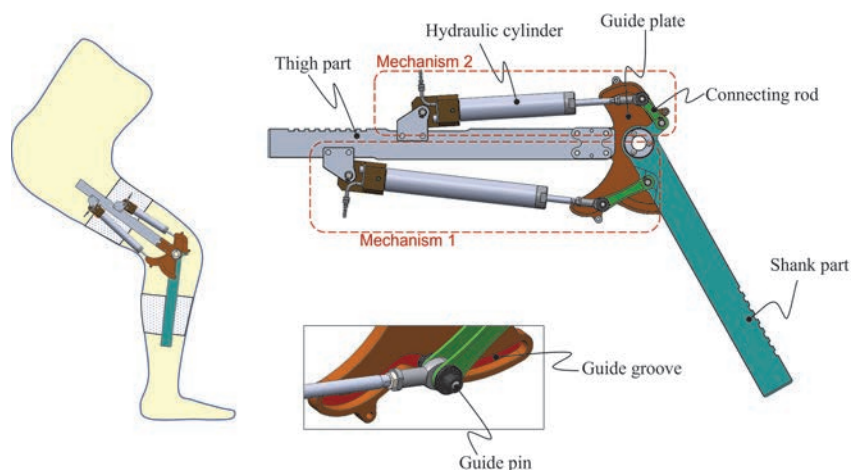


Figure 1 Knee exoskeleton device attached to the human leg and the upper guide plate removed to reveal the details of its internal components. The inset at the bottom shows the guide groove and guide pin.

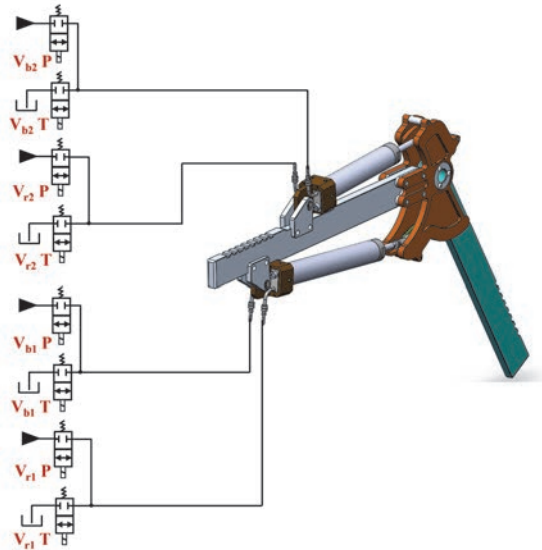


Figure 2 Hydraulic system of the knee exoskeleton. In valve identifiers, P and T represent the valves connected to the pressure source and tank, respectively, and indices b and r represent the valves connected to the bore and rod side chambers, respectively.

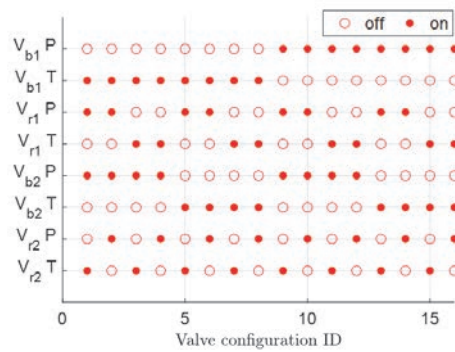


Figure 3 Valve positions for 16 valve configurations.

In this hydraulic system, there are 16 different valve configurations that result in each of the 4 hydraulic chambers in the two cylinders connected to either the pressure source or tank (Figure 3). Thus, there are 16 discrete force levels delivered by this hydraulic drive.

2.2 Transmission Ratios and Effective Force

The transmission ratio of the mechanisms in the knee exoskeleton device is defined as the ratio of the linear motion of the hydraulic cylinder and the angular motion of the knee joint:

$$T_{R,1,2} = \frac{dz_{1,2}}{d\psi} \quad (1)$$

where, z is the piston position in the hydraulic cylinder and ψ is the knee angle (Figure 4). The transmission ratio establishes the relationship between the forces from the hydraulic cylinders and the torque at the knee joint [13]:

$$M = T_{R,1}F_1 + T_{R,2}F_2 \quad (2)$$

where the cylinder force is determined from the pressure forces at bore and rod sides:

$$F = p_b A_b - p_r A_r \quad (3)$$

A key requirement of the knee exoskeleton device is to deliver the torque required in a typical gait cycle. To determine this torque requirement, the human motion dynamics data from HuMoD database [16, 17] are utilized. The motion data from this resource are used in a multi-body numerical model of lower limb (details of which are presented in Section 5.1) to obtain the knee torque. Figure 5(a) shows the variation of knee angle (ψ) and torque (M) over one gait cycle with 100 Nm being the peak torque.

It is notable that due to the digital nature of the hydraulic drive, the knee exoskeleton device provides the knee torque in a digital manner. To ensure that the steps in the torque generated are uniform, the area ratio of the hydraulic cylinders should be 4:1

$$A_b = 4A_r \quad (4)$$

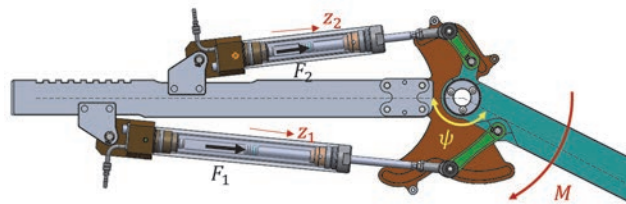


Figure 4 Illustration of piston position (z_1, z_2), knee angle (ψ), cylinder forces (F_1, F_2) and knee torque (M).

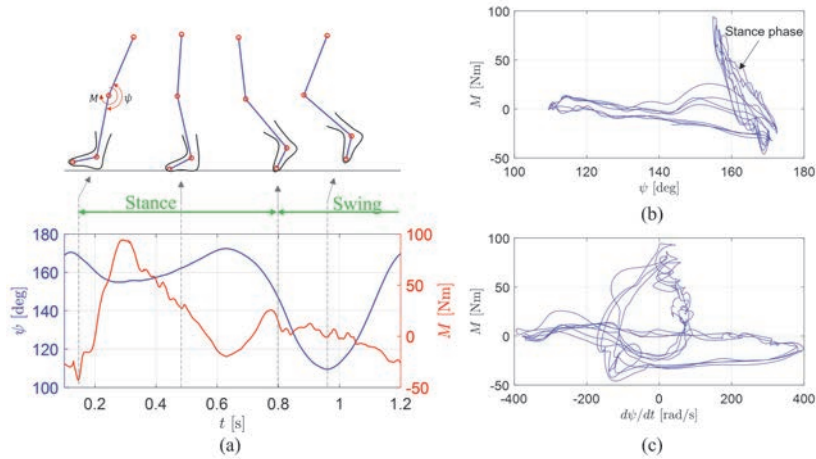


Figure 5 (a) Knee angle and torque over one gait cycle; (b) knee torque vs knee angle over multiple gait cycles; (c) knee torque vs knee angular speed over multiple gait cycles.

and the transmission ratio of the two mechanisms in the exoskeleton must differ by a factor of 2 [13].

$$T_{R,2} = -0.5T_{R,1} \quad (5)$$

Here, the negative sign accounts for the opposite motion of the pistons in the two mechanisms for a given knee motion.

From Equations (2)–(5), the torque delivered by the exoskeleton device simplifies to:

$$M = T_{R,1}A_b(p_{b1} - 0.25p_{r1} - 0.5p_{b2} + 0.125p_{r2}) \quad (6)$$

This expression helps in defining the effective force as:

$$F_{eff} = A_b(p_{b1} - 0.25p_{r1} - 0.5p_{b2} + 0.125p_{r2}) \quad (7)$$

Figure 6 confirms that the conditions on the area ratio (Equation (4)) and transmission ratio (Equation (5)) guarantee the uniform stepping of the effective force delivered by the drive.

3 Design Optimization Study

Design optimization study is a critical step in the design process to determine a (set of) design(s) that are optimal with respect to certain key factors (design

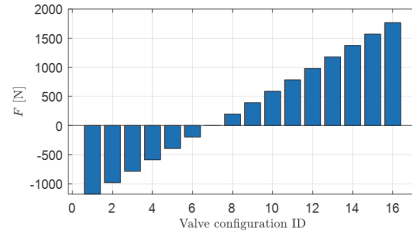


Figure 6 Effective force levels for 16 valve configurations (for $A_b = 78.54 \text{ mm}^2$ and source pressure of 200 bar).

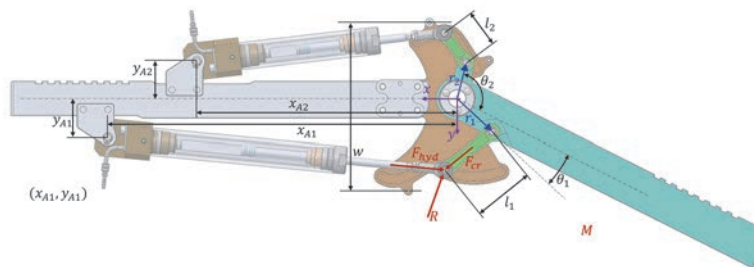


Figure 7 Nomenclature for defining the optimization problem.

criteria) while continuing to provide the basic functionalities the device was conceived for. This section details the optimization study performed on the knee exoskeleton device presented in the previous section.

3.1 Objective Functions

For users' comfort, the size and weight of the knee exoskeleton are critical factors. In the exoskeleton design conceived by the authors, the lateral dimension (referred to as device width and shown as w in Figure 7) should not extend the width of the knee and ideally should be as small as possible. Furthermore, the size of the cylinders (i.e., diameter and length) should be as small as possible too.

For a given exoskeleton design, the maximum distance between the guide curves essentially dictates the device width. Thus, if B_1 and B_2 represent the guide curves, the first objective function is:

$$\text{OF1 : minimize } w; \quad w = \max |y_{B1}| + \max |y_{B2}| \quad (8)$$

Next, the cylinder size is influenced by its bore diameter and the piston stroke during operation. Thus, minimization of cylinder size translates to the minimization of bore diameter and piston stroke.

For bore diameter minimization, the relationship between the cylinder chamber pressures and knee torque needs to be examined. From Equation (6), the maximum torque is delivered when the bore side chamber of cylinder 1 and rod side chamber of cylinder 2 are connected to the supply pressure ($p_{b1} = p_{r2} = p_S$) and the other chambers are connected to the tank ($p_{b1} = p_{r2} = 0$). Consequently, the cylinder bore area is

$$A_b = \frac{M_{max}(\psi)}{1.125 p_S T_{R,1}(\psi)} \quad (9)$$

where $M_{max}(\psi)$ is the maximum torque required at a given knee angle ψ (Figure 5(b)) and $T_{R,1}(\psi)$ is determined from the design variables (Section 3.2). Thus, the third objective function is:

$$\text{OF2 : minimize } d_b; \quad d_b = \sqrt{\frac{4}{\pi} \max \left(\frac{M_{max}(\psi)}{1.125 p_S T_{R,1}(\psi)} \right)} \quad (10)$$

The objective function related to stroke minimization can be determined directly from the definition of transmission ratio (Equation (1)):

$$\text{OF3 : minimize } S_1; \quad S_1 = \int_{\psi_1}^{\psi_2} T_{R,1}(\psi) d\psi \quad (11)$$

where, $[\psi_1, \psi_2]$ is the knee angle range. It is notable that Equation (5) establishes that the stroke of cylinder 2 is always half of cylinder 1. Thus, cylinder 2 stroke minimization does not require an additional objective function.

Finally, in the exoskeleton design, at the guide pins, the lateral components of the forces from the hydraulic cylinder (F_{hyd}) and connecting rod (F_{cr}) need to be supported by the grooves on the guide plates (as illustrated for mechanism 1 in Figure 7). For compact and lightweight design, it is desirable to have relatively thin and light guide plates. To ensure this, the contact force (R) must be as low as possible. In fact, keeping this force low also helps with minimizing the friction force at the guide pins (thus, improving the overall efficiency of the exoskeleton device). Thus, minimizing the contact force at the guide pins forms the fourth objective of the optimization study.

To quantify this objective, the knee torque and transmission ratio information is used to calculate the hydraulic force at the cylinders and then the

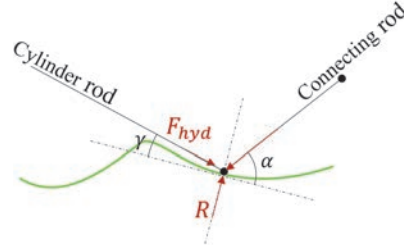


Figure 8 Calculation of the contact force at the guide groove.

contact force at the guide groove is evaluated as

$$R = F_{hyd}(\sin \gamma + \cos \gamma \tan \alpha) \quad (12)$$

where, γ is the angle between the cylinder rod and the tangent to the guide groove at the pin-joint location (Figure 8). Similarly, α is the angle between the connecting rod and the tangent to the guide groove. The objective is then to minimize the maximum value of R for the two mechanisms over a gait cycle:

$$\text{OF4: minimize } R_{max}; \quad R_{max} = \max(R_1, R_2) \quad (13)$$

3.2 Design Variables

The design variables for the optimization study are the dimensions $r_1, r_2, l_1, l_2, x_{A1}, y_{A1}, x_{A2}, y_{A2}, \theta_1, \theta_2$ as indicated in Figure 7. Furthermore, as the nature of the guide curves is influenced by the choice of transmission ratio, the transmission ratio is also a design variable. It is notable that the nature of the guide curve allows a variable transmission ratio over the knee angle range. Thus, the transmission ratio design variable is in fact a set of eight real numbers that correspond to the transmission ratio at knee angles $\psi = \{120^\circ, 125^\circ, \dots, 150^\circ, 155^\circ\}$. The transmission ratio at the intermediate knee angles are determined via shape-preserving piecewise cubic interpolation [18]. Outside of this angle range, the end values are used, i.e. the transmission ratio stays constant for $\psi > 155^\circ$ and $\psi < 120^\circ$.

For $\psi > 155^\circ$, a constant transmission ratio ensures a linear relationship between (a) the knee torque and hydraulic force, and (b) the knee angle and piston position. Furthermore, in the stance phase (where $\psi \in [155^\circ, 175^\circ]$), a linear relationship exists between the knee torque and knee angle (Figure 5(b)). These linearities result in a linear relationship between the hydraulic pressure in the cylinder chamber and piston position which

allows a passive control of knee exoskeleton in the stance phase (details of which is present in Section 4.1).

3.3 Design Constraints

For the design to be feasible, manufacturable, and operable, the design must satisfy the following constraints:

- The design must be kinematically feasible for the full range of knee motion.
- During the full range of knee motion, different parts of the exoskeleton device must not interfere. This includes the possible interference between (a) the cylinders and the thigh part, (b) cylinder rod 2 and knee joint, and (c) connecting rod 2 and knee joint.
- The curvature of the guide curves should be smaller than a prescribed value (170 m^{-1} is considered as an appropriate limit). This constraint has implications on the real manufactured part. In the manufactured part, the guide curve forms a groove in which the guide pin moves. If the curvature of the groove becomes too high, the knee motion may experience a jerky behaviour when the guide pin passes through this region. This constraint aims to avoid this possibility.
- The lateral dimension of the exoskeleton in the direction towards the front of the knee is particularly undesirable as it extends out of the body contour. As the guide curve B_2 is towards the front of the knee, the following constraint is enforced: $|y_{B2}| < 5.5 \text{ cm}$.

3.4 Optimization Procedure and Results

The optimization problem is solved in MATLAB environment using NSGA-II algorithm which is well suited for multi-objective optimizations [19]. The initial design space is populated with 5000 designs and the optimization algorithm is executed for 500 generations.

Figure 9 shows the approximate pareto front obtained from the optimization where three objective functions are displayed on the three coordinate axes and the device width objective function is displayed by the color of the markers. The figure indicates that no design performs the best in regards to all of the objectives.

To better understand the relationship between the objectives, plots between each pair of objectives are presented in Figure 10. The correlation between the objective pairs is quantified via the correlation coefficient which

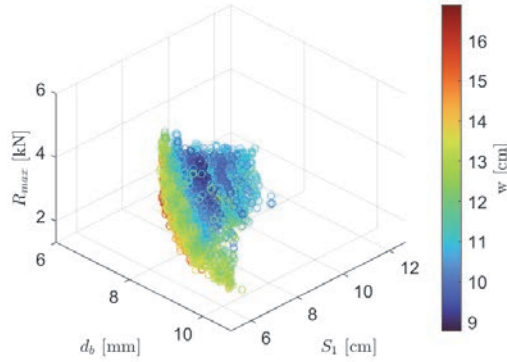


Figure 9 Pareto front obtained from the optimization.

for two datasets x and y is defined as:

$$c_{xy} = \frac{1}{n-1} \sum_{i=1}^n \left(\frac{x_i - \bar{x}}{\sigma_x} \right) \left(\frac{y_i - \bar{y}}{\sigma_y} \right) \quad (14)$$

where, $\bar{}$ and σ are the mean and standard deviation of the dataset, respectively.

In Figure 10, the diagonal plots exhibit the most significant correlations. Firstly, a strongly inverse relationship between the cylinder bore diameter and stroke is observed which is expected since the transmission ratio (a design variable) appears in the denominator of OF2 expression (Equation (10)) and numerator of OF3 expression (Equation (11)). Next, an inverse relationship between the piston stroke and contact force is observed. This is explained from the fact that a higher stroke is indicative of a higher transmission ratio which leads to a lower hydraulic force (F_{hyd}) for a given knee torque, and in turn to a lower contact force. Finally, an inverse relationship between the device size and contact force is observed. This is due to the fact that as the device size increases, the guide curve has more freedom to arrive at a position and curvature that allows lower values of the angle between the connecting rod and guide curve (α in Figure 8), resulting in a lower contact force.

3.5 Reduction of Objective Function Dimensionality

Since no one design performs the best in regards to all the design objectives, choosing a design from a four-dimensional pareto-front is challenging. To address this, certain logical decisions are made. Firstly, if increasing the

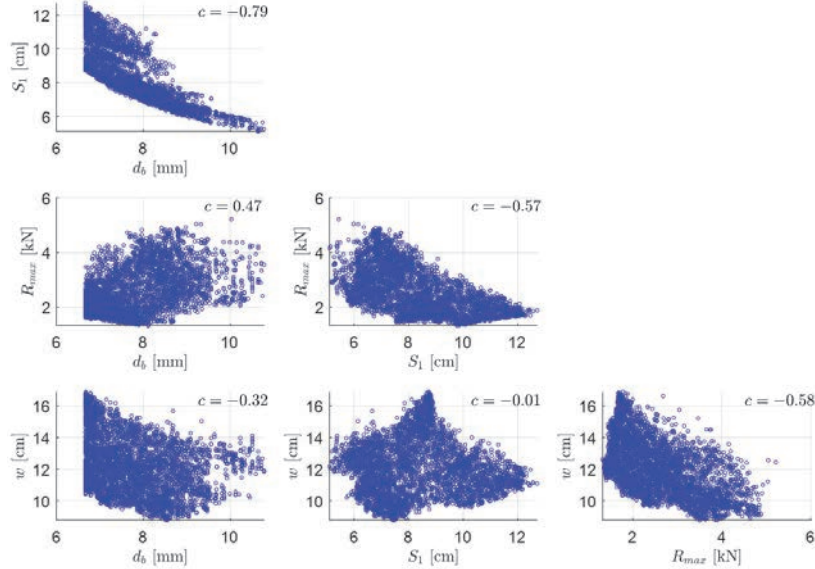


Figure 10 Relationships between objective function pairs. The correlation coefficient c is indicated in top right of each figure.

cylinder diameter by few millimeters helps in other objectives (particularly reducing the device width and piston stroke in the order of centimeters as observed in Figure 10), it makes sense to relax this objective. Furthermore, the hydraulic cylinders are only available for certain whole-number values of bore diameters. Thus, cylinder bore diameter of 10 mm is chosen.

Next, as the cylinders are in line with the thigh, slightly longer cylinders can be tolerated if that helps with the device width and contact force objectives. Thus, the stroke objective is converted into a constraint:

$$\text{Constraint: } S_1 < 8 \text{ cm} \quad (15)$$

This reduces the dimensionality of the objective function space to two (with the two objective functions being the minimization of device width and contact force). The new optimization problem with two objectives and an additional constraint is again solved using NSGA-II algorithm (2000 initial population designs and 1000 generations).

The approximate pareto-front obtained from the optimization is shown in Figure 11. An inverse relationship between the device width and contact force is again observed. The design indicated in red has the lowest contact

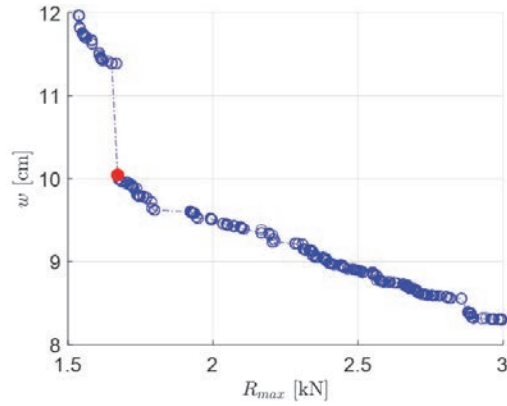


Figure 11 2D Pareto-front obtained from the optimization.

Table 1 Design variable values for the selected design

r_1	37 mm	r_2	29 mm	l_1	34 mm
l_2	32 mm	x_{A1}	251 mm	y_{A1}	32 mm
x_{A2}	178 mm	y_{A2}	36 mm	θ_1	47°
θ_2	164°				

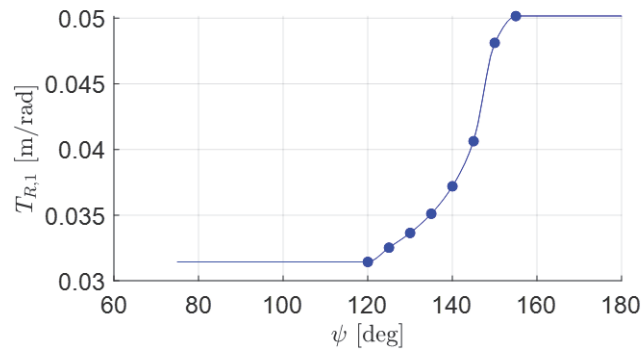


Figure 12 Transmission ratio of mechanism 1 of the selected design. The eight design variables that form the transmission ratio curve are indicated as filled circles.

force without a significant increase in the device width. Thus, this design is chosen from the optimization study.

The values of the design variables (except the transmission ratio) for the selected design are reported in Table 1. The transmission ratio ($T_{R,1}$) for the selected design is shown in Figure 12. The increment of the transmission ratio

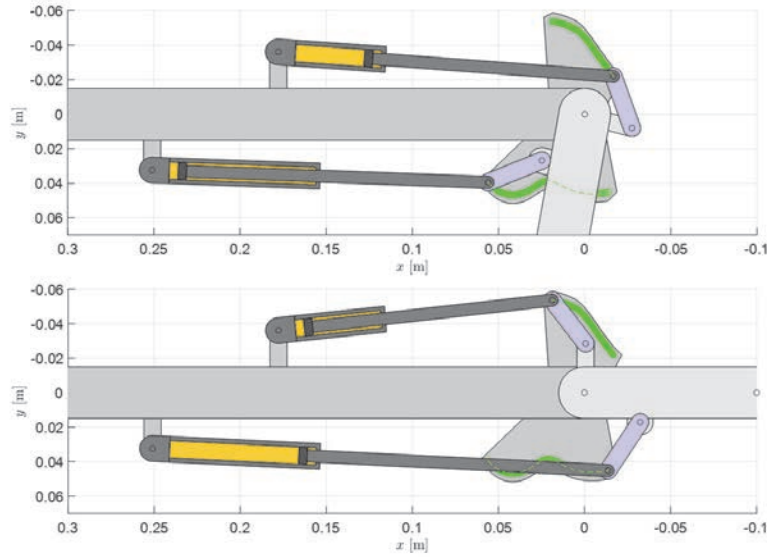


Figure 13 Selected exoskeleton design in flexion and extension positions. The guide curves are shown in green.

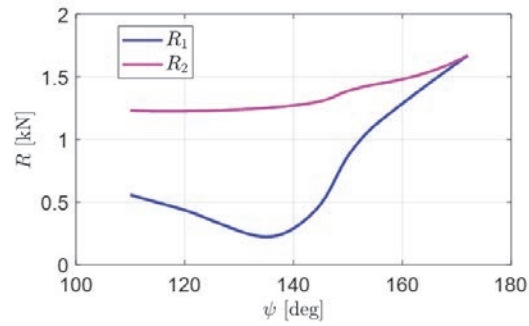


Figure 14 Contact force at the mechanism guide curves for the selected design.

with knee angle in the range $[120^\circ, 155^\circ]$ is expected since the knee torque increases with knee angle in this range (Figure 5(b)).

Figure 13 shows the chosen exoskeleton design for two extreme positions (flexion and extension), and Figure 14 shows the contact force at the guide curves over the knee angle range of a typical gait cycle.

4 Control Strategy

A critical requirement of the knee exoskeleton device is that it should follow the pattern involved in the natural walking cycle while also providing the required knee torque. In this section, a control strategy is proposed that can fulfil this requirement efficiently. Different methods are used for the stance and swing phases of the gait cycle and these methods are described in the following subsections.

4.1 Stance Phase

Upon careful examination of the limb motion in a typical gait cycle and the required torque at the knee (Figure 5), it is observed that in the stance phase, the knee torque – angle characteristic resembles an elastic behaviour. As shown in Figure 5(b), the knee torque, M increases (approximately linearly) with decrease in the knee angle ψ , and vice versa. This peculiar characteristic allows a passive control of the knee motion during the stance phase with the fluid in the hydraulic system acting as the elastic element (via its compressibility).

To achieve this, V_{b1} and V_{r2} chambers of the hydraulic cylinders (Figure 15) are blocked, i.e., all the valves connected to these chambers are

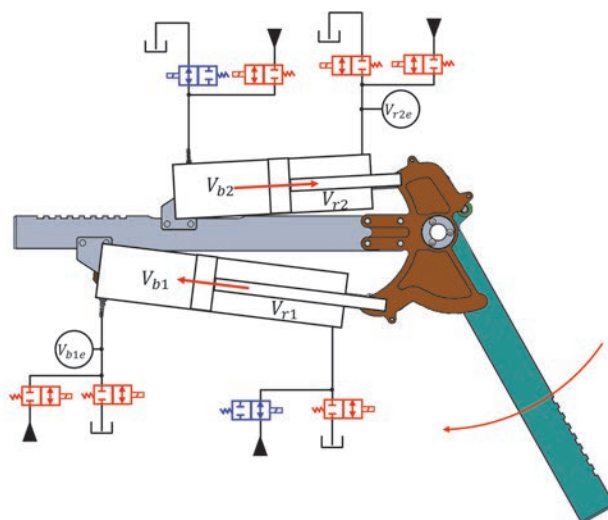


Figure 15 The valve configuration during the stance phase: red valves are closed, blue valves are open.

turned off. Thus, at the beginning of the stance phase, when the knee angle decreases, these volumes get compressed, resulting in the rise of pressures in these chambers. The forces from these pressures support the increasing knee torque in this phase. The opposite happens when the knee angle subsequently decreases.

The volume of fluid required to realize this elastic behaviour depends on the bulk modulus of the fluid, the air content in the fluid, and the peak torque requirement in the elastic phase. To account for possible variations in these factors, the valve manifold design will have necessary attachments that can allow additional variable fluid volumes in the hydraulic circuit (V_{b1e} and V_{r2e} shown in Figure 15) as per the elasticity requirement.

A key advantage of this passive control during the stance phase is its simplicity. Furthermore, as 6 out of 8 valves stay closed in this phase and the rest of 2 valves do not undergo any switching, the energy losses at the valves are significantly lower.

4.2 Swing Phase

In the swing phase, the tracking of the knee motion does not need to be very accurate. However, it is important that the knee angle does not veer away so much (from the natural trajectory) to risk contact between the foot and the ground. Furthermore, the knee angle must reach the required angular position at the beginning of the stance phase. To achieve these requirements, a simplified form of model predictive control is employed.

This control method is illustrated via Figure 16. At a time t_n , the actual knee angle is $\psi_{a,n}$ and the valve command u for the next time step (t_n to t_{n+1}) is needed to be determined. A valve command is essentially a set of commands (on/off) to each of the 8 valves in the hydraulic circuit. The current knee angle state ($\psi_{a,n}, \dot{\psi}_{a,n}$) and the desired knee angle state at the next time step ($\psi_{d,n+1}, \dot{\psi}_{d,n+1}$) are used to determine a knee angle path described by a third order polynomial in time. From this polynomial, the knee angular position, speed, and acceleration at $t_m = 0.5(t_n + t_{n+1})$ is used in a mechanical model of limb motion to determine the required knee torque. The details of this mechanical model are presented in Section 5.1. From this required knee torque and transmission ratio information, the effective force requirement is determined. Using the effective force vs valve configuration ID data (Figure 6), a valve configuration is chosen that brings the digital force level closest to this desired force. This valve configuration is the control output for the next time step.

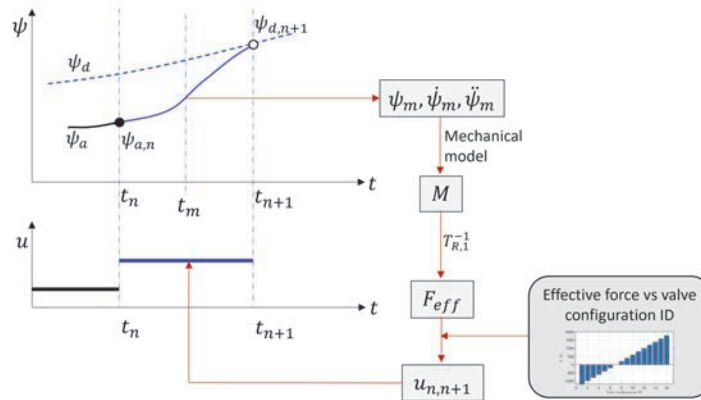


Figure 16 Illustration of the simplified form of model predictive control.

Near the end of the swing phase ($t \in [1 \text{ s}, 1.2 \text{ s}]$ in Figure 5(a)), the knee angle increases rapidly. This results in a rapid rise in the volume of V_{b1} chamber (Figure 15) and consequently, a rapid fall in the chamber pressure. At low pressures, the hydraulic fluid's compressibility increases significantly. Going into the next stance phase with such a compressible volume, the device will fail to supply the necessary torque at the beginning of the stance phase. To avoid this potential problem, near the end of the swing phase, the controller commands a valve configuration that allows V_{b1} chamber to be connected to the pressure source for a brief amount of time, raising the pressure in this chamber to an appropriate level.

5 Numerical Model of Knee Exoskeleton

To study the behavior of the knee exoskeleton design and control strategy presented in the previous sections, a numerical model of the human limb and knee exoskeleton previously developed by the authors is used. A brief description of the model is provided in this section.

5.1 Mechanical Model of Limb Motion

The mechanical model of limb motion consists of a planar model comprising foot, shank, and thigh (Figure 17). The motion of the upper body until thigh is considered to be known (from HuMoD database) and thus, the system has only 2 degrees of freedom: angular motion of shank and foot.

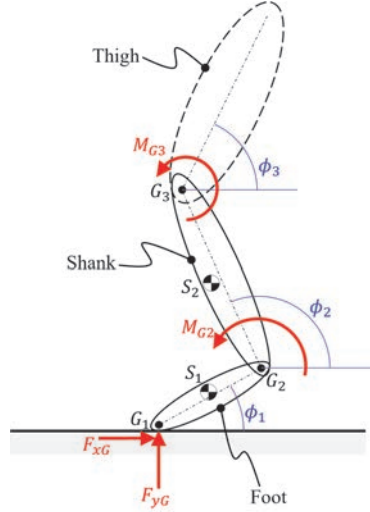


Figure 17 Planar view of limb with variables present in the mechanical model.

The kinetic and potential energy of the system can be expressed as:

$$T = \frac{1}{2} \sum_{i=1}^2 (m_i \dot{\mathbf{x}}_{S_i} \cdot \dot{\mathbf{x}}_{S_i} + J_i \dot{\phi}_i^2) \quad (16)$$

$$V_p = g \sum_{i=1}^2 m_i \mathbf{x}_{S_i} \cdot \mathbf{e}_y \quad (17)$$

where, m_i is the mass, \mathbf{x}_{S_i} is the position of the center of mass, J_i is the moment of inertia, ϕ_i is the angular position of the i^{th} limb part and \mathbf{e}_y is the unit vector in vertical direction.

Next, the virtual work due to the torques at the joints (M_{G_i}) and the ground reaction force (\mathbf{F}_G) is:

$$\delta W = \sum_{i=2}^3 M_{G_i} (\delta \phi_i - \delta \phi_{i-1}) + \mathbf{F}_G^T \delta \mathbf{x} \quad (18)$$

Substituting these expressions into the Lagrange equation of motion and simplifying, the following expression for shank motion is obtained:

$$m_{eff,2} \ddot{\phi}_2 = -m_{eff,1} \ddot{\phi}_1 + M_{hyd} + \mathbf{k} \mathbf{B}_F \mathbf{F}_G + \mathbf{k} \mathbf{V}_{f0} \quad (19)$$

where, $m_{eff,1}$ and $m_{eff,2}$ are the effective masses of foot and shank, M_{hyd} is the knee torque (that is supplied by the exoskeleton device), $k\mathbf{B}_F\mathbf{F}_G$ is the ground reaction term and $k\mathbf{V}_{f0}$ contains the terms related to the centripetal force, gravity, and the force from thigh. The complete expressions are lengthy and hence, are not shown here.

5.2 Hydraulic Model

The pressures in the cylinder chambers are modelled using the pressure build up equation:

$$\frac{dp_i}{dt} = \frac{K(p)}{V_i} \left(Q_i - A_i \frac{dz_i}{dt} \right) \quad (20)$$

where, $K(p)$ is pressure dependent bulk modulus of the fluid, Q_i is the flow entering the i^{th} chamber, V_i is the volume of the i^{th} chamber, A_i is the cross-sectional area of the i^{th} chamber and dz_i/dt is the speed of the piston (positive for the expanding chamber and negative for the contracting chamber).

The flow through the valves is modelled using the orifice equation

$$Q_{i,P/T} = \text{sign}(p_i - p_{P/T}) y_{i,P/T} Q_N \sqrt{\frac{|p_i - p_{P/T}|}{p_N}} \quad (21)$$

where, Q_N and p_N are the nominal flow rate through and nominal pressure drop across the valves, respectively and y_i is the position of the i^{th} valve ($0 \leq y_i \leq 1$).

6 Simulation Results and Discussion

The numerical model presented in Section 5 is used to simulate a typical gait cycle. The design selected from the optimization study in Section 3 is used in the simulation study and the control strategy described in Section 4 is employed. Limb parameters of subject B from the HuMoD database are used and the performance of the exoskeleton device is evaluated against the natural walking pattern of this subject. The subject is a central European male who is 32 years old, 1.79 m tall and weighs 84.8 kg. The details of his limb parameters are reported in Table 2.

In the simulations, all of the knee torque is assumed to be provided by the exoskeleton, i.e., the user does not contribute any torque. Moreover, the

Foot Parameters	Values	Shank Parameters	Values
Length	0.165 m	Length	0.432 m
Mass	1.006 kg	Mass	4.037 kg
Moment of inertia	0.006 kg m ²	Moment of inertia	0.058 kg m ²

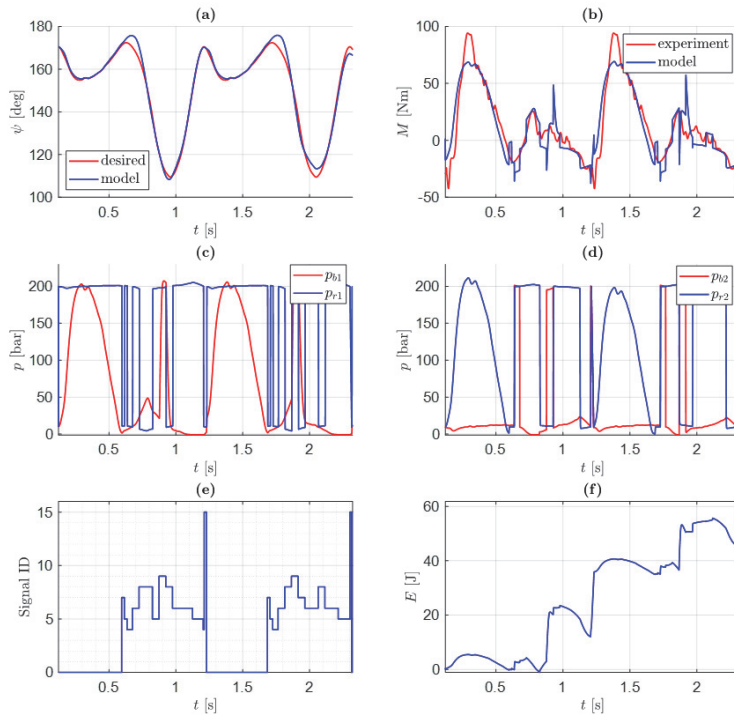


Figure 18 (a) Knee angle comparison between the model and the desired behaviour; (b) comparison between the knee torque obtained from the model and the measurements; (c) pressure in the chambers of the hydraulic cylinder 1; (d) pressure in the chambers of the hydraulic cylinder 2; (e) signal ID of the valve configuration commanded by the controller; (f) energy consumption over two gait cycles.

pressure levels at the pressure source and tank are considered to be 200 bar and 10 bar, respectively.

Figure 18 shows the results for two gait cycles. The knee angle obtained from the simulation results are shown to track the desired motion reasonably

well. The maximum deviation between the desired and simulated knee angle is 7° . Experimental tests planned in the future will include the investigation of the effect of such deviations on the user comfort.

Figure 18(b) shows that the exoskeleton device is successfully able to provide the required torque over the gait cycles. Figure 18(c) and 18(d) show the pressures in the chambers of hydraulic cylinders. The stance phase is identifiable from the gradual rise and subsequent fall of pressures (p_{b1} and p_{r2}) in the chambers that are blocked during this phase.

Figure 18(e) shows the signal ID of the valve configuration commanded by the controller. ID value of 0 indicates the configuration where all the valves for V_{b1} and V_{r2} chambers are closed. This configuration is commanded in the stance phase of the gait cycle. ID values of 1 to 16 corresponds to 16 configurations described in Figure 3, out of which, appropriate configurations are chosen by the model predictive control algorithm in the swing phase. Near the end of swing phase, signal ID of 15 is commanded to allow V_{b1} connection to the pressure source to avoid the high compressibility issue (discussed in Section 4.2).

Lastly, Figure 18(f) shows the energy consumed by the exoskeleton device over two gait cycles. The energy consumed per cycle is 30 joules. The dominating part of this consumption occurs when the volume V_{b1} is pressurized at the end of the swing phase. The magnitude of this consumption is dependent on the compressibility behaviour of the fluid at low pressures which is significantly influenced by the amount of air present in the fluid. The energy consumption could be reduced by using a large check valve between the volume V_{b1} and the tank to allow the suction of the fluid into the volume when the pressure in the volume falls below the tank pressure. However, such a solution will negatively impact the compactness of the device, and so, the overall advantage of such a solution (or other alternatives) needs to be further investigated.

7 Summary and Conclusion

This article presents an optimal design of digital hydraulically driven knee exoskeleton and an efficient strategy to control its motion. Firstly, with the goal of determining a compact lightweight exoskeleton design, a multi-objective design optimization study is performed. The study demonstrates various tradeoffs between different design objectives. Based on component availability and user comfort, key design decisions are made that reduce the pareto-front dimensionality to two from which the optimal design is chosen.

Secondly, on the control side, a passive control of the exoskeleton device during the stance phase of gait cycle is proposed. This is an energy efficient strategy as the losses associated with the valve actuation and short-circuited flow during valve position changes are eliminated. For the swing phase, a simplified form of model predictive control is implemented to allow the tracking of knee motion in a computationally efficient manner.

The performance of the exoskeleton design and the control strategy presented in this work is analyzed via a numerical model of the knee exoskeleton and human limb. The results indicate that the exoskeleton device is successfully able to track the motion of the knee in a typical gait cycle and supply the required torque. A major source of energy consumption is found to be the pressurization of one of the cylinder chambers at the beginning of the gait cycle. Strategies to minimize this energy consumption will be investigated in future.

Acknowledgements

This work was done in the framework of the COMET K2 Center on Symbiotic Mechatronics, which is funded by the Austrian Federal Government, the State Upper Austria and by its Scientific and Industrial Partners.

Nomenclature

A	Area
c	Correlation coefficient
d	Diameter
E	Energy
F	Force
g	Acceleration due to gravity
J	Moment of inertia
K	Bulk modulus of the fluid
l	Connecting rod length
M	Knee torque
m	Mass
p	Pressure
Q	Flow rate
R	Contact force at the guide curve
r	Crank radius
S	Piston stroke

T	Kinetic energy
T_R	Transmission ratio
u	Valve command
t	Time
V	Volume
V_p	Potential energy
w	Lateral width of the exoskeleton device
x, y	Cartesian coordinate positions
z	Piston position in the hydraulic cylinder

Greek letters

α	Angle between the connecting rod and tangent to the guide groove at pin joint
γ	Angle between the cylinder rod and tangent to the guide groove at pin joint
θ	Angle between the crank and the shank part
σ	Standard deviation
ϕ	Angular position of the limb part
ψ	Knee angle

Subscripts

1, 2	Mechanism identifier
A	Cylinder base joint
a	Actual
B	Guide curve
b	Bore side of hydraulic cylinder
cr	Connecting rod
d	Desired
e	Extra
eff	Effective
hyd	Hydraulic
m	Mean
N	Nominal
n	time step identifier
P	Pressure source
r	Rod side of hydraulic cylinder
S	Supply
T	Tank

Acronyms

OF	Objective function
----	--------------------

References

- [1] J.A. de la Tejera, R. Bustamante-Bello, R.A. Ramirez-Mendoza, J. Izquierdo-Reyes, Systematic Review of Exoskeletons towards a General Categorization Model Proposal, *Appl. Sci.* 11 (2021) 76. <https://doi.org/10.3390/app11010076>.
- [2] R. Scheidl, Digital fluid power for exoskeleton actuation – guidelines, opportunities, challenges, in: *Ninth Workshop Digit. Fluid Power*, Aalborg, Denmark, 2017.
- [3] H. Kazerooni, J.-L. Racine, L. Huang, R. Steger, On the Control of the Berkeley Lower Extremity Exoskeleton (BLEEX), in: *Proc. 2005 IEEE Int. Conf. Robot. Autom.*, 2005: pp. 4353–4360. <https://doi.org/10.1109/ROBOT.2005.1570790>.
- [4] J. Ghan, R. Steger, H. Kazerooni, Control and system identification for the Berkeley lower extremity exoskeleton (BLEEX), *Adv. Robot.* 20 (2006) 989–1014. <https://doi.org/10.1163/156855306778394012>.
- [5] A.B. Zoss, H. Kazerooni, A. Chu, Biomechanical design of the Berkeley lower extremity exoskeleton (BLEEX), *IEEEASME Trans. Mechatron.* 11 (2006) 128–138. <https://doi.org/10.1109/TMECH.2006.871087>.
- [6] W. Huo, S. Mohammed, J.C. Moreno, Y. Amirat, Lower Limb Wearable Robots for Assistance and Rehabilitation: A State of the Art, *IEEE Syst. J.* 10 (2016) 1068–1081. <https://doi.org/10.1109/JSYST.2014.2351491>.
- [7] Y. Yang, X. Dong, X. Liu, D. Huang, Robust Repetitive Learning-Based Trajectory Tracking Control for a Leg Exoskeleton Driven by Hybrid Hydraulic System, *IEEE Access.* 8 (2020) 27705–27714. <https://doi.org/10.1109/ACCESS.2020.2971777>.
- [8] J. Jiang, Y. Wang, H. Cao, J. Zhu, X. Zhang, A novel pump-valve coordinated controlled hydraulic system for the lower extremity exoskeleton, *Trans. Inst. Meas. Control.* 42 (2020) 2872–2884. <https://doi.org/10.1177/0142331220930623>.
- [9] T. Kosaki, S. Li, A Water-Hydraulic Upper-Limb Assistive Exoskeleton System with Displacement Estimation, *J. Robot. Mechatron.* 30 (2020) 149–156.
- [10] R. Scheidl, M. Linjama, S. Schmidt, Is the future of fluid power digital?, *Proc. Inst. Mech. Eng. Part J. Syst. Control Eng.* 226 (2012) 721–723. <https://doi.org/10.1177/0959651811435628>.
- [11] H. Cao, Z. Ling, J. Zhu, Y. Wang, W. Wang, Design frame of a leg exoskeleton for load-carrying augmentation, in: *2009 IEEE Int. Conf. Robot. Biomim. ROBIO*, 2009: pp. 426–431. <https://doi.org/10.1109/ROBIO.2009.5420684>.

- [12] E. Holl, R. Scheidl, S. Eshkabilov, Simulation Study of a Digital Hydraulic Drive for a Knee Joint Exoskeleton, in: Proc. ASMEBATH 2017 Symp. Fluid Power Motion Control, Sarasota, Florida, USA, 2017. <https://doi.org/10.1115/FPMC2017-4220>.
- [13] R. Rituraj, R. Scheidl, P. Ladner, M. Lauber, A Novel Design Concept of Digital Hydraulic Drive for Knee Exoskeleton, in: Proc. ASMEBATH 2021 Symp. Fluid Power Motion Control, Virtual, Online, 2021. <https://doi.org/10.1115/FPMC2021-68590>.
- [14] HAWE Micro Fluid GmbH, (2022). www.hawe.com.
- [15] M. Linjama, M. Paloniitty, L. Tiainen, K. Huhtala, Mechatronic Design of Digital Hydraulic Micro Valve Package, *Procedia Eng.* 106 (2015) 97–107. <https://doi.org/10.1016/j.proeng.2015.06.013>.
- [16] J. Wojtus, O. von Stryk, HuMoD – A versatile and open database for the investigation, modeling and simulation of human motion dynamics on actuation level, in: 2015 IEEE-RAS 15th Int. Conf. Humanoid Robots Humanoids, 2015: pp. 74–79. <https://doi.org/10.1109/HUMANOIDS.2015.7363534>.
- [17] HuMoD, (n.d.). <https://www.sim.informatik.tu-darmstadt.de/res/ds/humod/>.
- [18] F.N. Fritsch, R.E. Carlson, Monotone Piecewise Cubic Interpolation, *SIAM J. Numer. Anal.* 17 (1980) 238–246. <https://doi.org/10.1137/0717021>.
- [19] K. Deb, A. Pratap, S. Agarwal, T. Meyarivan, A fast and elitist multiobjective genetic algorithm: NSGA-II, *IEEE Trans. Evol. Comput.* 6 (2002) 182–197. <https://doi.org/10.1109/4235.996017>.

Biographies



Rituraj received his B.Tech. degree from IIT Guwahati, India in 2013 and his Ph.D. degree from Purdue University, USA in 2020. During his direct-Ph.D.

at Maha Fluid Power Research Center, he worked on numerical modelling of External Gear Machines. Currently, he is a postdoctoral researcher at Institute of Machine Design and Hydraulic Drives in JKU, Austria where he is working on the development of hydraulically driven exoskeletons. His overall research interests include numerical and experimental study of hydraulic components and systems.



Rudolf Scheidl received his M.Sc. of Mechanical Engineering and Doctor of Engineering Sciences degrees at Vienna University of Technology. He has research and development experience in agricultural machinery (Epple Buxbaum Werke), continuous casting technology (Voest-Alpine Industrieanlagenbau) and paper mills (Voith). Since 1990, he is a full Professor of Mechanical Engineering at Johannes Kepler University, Austria. His research topics include hydraulic drive technology and mechatronic design.

